Quantum Science and Technology

PAPER

A method for controlling the magnetic field near a superconducting boundary in the ARIADNE axion experiment

H Fosbinder-Elkins[1,10,12], Y Kim[2,3,12], J Dargert[1], M Harkness[1], A A Geraci[4,*], E Levenson-Falk[5,13], S Mumford[6], A Fang[7], A Kapitulnik[7], A Matlashov[2], D Kim[2,3], Y Shin[3], Y K Semertzidis[2,3], Y-H Lee[8], N Aggarwal[4], C Lohmeyer[4], A Reid[9,11], J Shortino[9], I Lee[9], J C Long[9], C-Y Liu[9] and W Snow[9]

[1] Department of Physics, University of Nevada, 1664 N Virgina St., Reno, 12, NV 89557, United States of America
[2] Department of Physics, KAIST, 291 Daehak-Ro, Daejeon 34141, Republic of Korea
[3] Center for Axion and Precision Physics Research, IBS, 193, Munji-Ro, Daejeon 34051, Republic of Korea
[4] Center for Fundamental Physics, Department of Physics and Astronomy, Northwestern University, Evanston, IL 60208, United States of America
[5] Department of Physics and Astronomy, University of Southern California, 825 Bloom Walk, Los Angeles, CA 90089, United States of America
[6] Physics Department, Stanford University, 382 Via Pueblo, Stanford, CA 94305, United States of America
[7] Department of Physics and Applied Physics, Stanford University, 382 Via Pueblo, Stanford, CA 94305, United States of America
[8] KRISS, 267 Gajeong-ro, Yuseong-gu, Daejeon 34113, Republic of Korea
[9] Department of Physics, Indiana University, 727 E Third St, Bloomington, IN 47405, United States of America
[*] Author to whom any correspondence should be addressed.
[10] Present address: Physics Department, University of Chicago, Chicago, IL.
[11] Present address: Department of Physics, Trinity College, Hartford, CT, United States of America.
[12] These authors contributed equally to this work.
[13] Former address: Physics Department, Stanford University, 382 Via Pueblo, Stanford, CA 94305.

E-mail: andrew.geraci@northwestern.edu

Keywords: dark matter, axion, superconducting magnetic shielding, quantum sensors

OPEN ACCESS

RECEIVED
22 October 2020

REVISED
15 March 2021

ACCEPTED FOR PUBLICATION
23 March 2021

PUBLISHED
6 January 2022

Abstract

The QCD axion is a particle postulated to exist since the 1970s to explain the strong-CP problem in particle physics. It could also account for all of the observed dark matter in the Universe. The axion resonant interaction detection experiment (ARIADNE) intends to detect the QCD axion by sensing the fictitious 'magnetic field' created by its coupling to spin. Short-range axion-mediated interactions can occur between a sample of laser-polarized ^{3}He nuclear spins and an unpolarized source-mass sprocket. The experiment must be sensitive to magnetic fields below the 10^{-19} T level to achieve its design sensitivity, necessitating tight control of the experiment's magnetic environment. We describe a method for controlling three aspects of that environment which would otherwise limit the experimental sensitivity. Firstly, a system of superconducting magnetic shielding is described to screen ordinary magnetic noise from the sample volume at the 10^8 level, which should be sufficient to reduce the contribution of Johnson noise in the sprocket-shaped source mass, expected to be at the 10^{-12} T$/\sqrt{\text{Hz}}$ level, to below the threshold for signal detection. Secondly, a method for reducing magnetic field gradients within the sample up to 10^2 times is described, using a simple and cost-effective design geometry. Thirdly, a novel coil design is introduced which allows the generation of fields similar to those produced by Helmholtz coils in regions directly abutting superconducting boundaries. This method allows the nuclear Larmor frequency of the sample to be tuned to match the axion field modulation frequency set by the sprocket rotation. Finally, we experimentally investigate the magnetic shielding factor of sputtered thin-film superconducting niobium on quartz substrates for various geometries and film thicknesses relevant for the ARIADNE axion experiment using SQUID magnetometry. The methods may be generally useful for magnetic field control near superconducting boundaries in other experiments where similar considerations apply.

1. Introduction

The axion resonant interaction detection experiment (ARIADNE) intends to search for the QCD axion using techniques based on nuclear magnetic resonance [1, 2]. Axions or axion-like particles will generically mediate short-range spin-dependent interactions between an ensemble of nuclear spins and an (un-polarized) attractor mass. In the experiment, a sample of laser-polarized ^{3}He nuclear spins feels a fictitious 'magnetic field' as the teeth of a sprocket-shaped tungsten attractor rotate past the sample at the nuclear Larmor precession frequency, set to be approximately 100 Hz (see figure 1) [2]. Here the axion is acting as the mediating boson responsible for the interaction. By choosing the size of the spin sample and attractor mass as well as their separation distance, different axion Compton wavelengths (masses) can be probed. Depending on the experimental configuration, the technique has the potential to probe deep within the theoretically interesting regime for the QCD axion in the mass range of 0.001–10 meV, while being independent of cosmological assumptions. Detecting the axion would explain the smallness of θ_{QCD} [3–6] and identify a component of dark matter [1, 5, 7].

The axion can mediate an interaction between fermions (e.g. nucleons) with a potential given by

$$U_{\mathrm{sp}}(r) = \frac{\hbar^2 g_{\mathrm{s}}^{\mathrm{N}} g_{\mathrm{p}}^{\mathrm{N}}}{8\pi m_{\mathrm{f}}} \left(\frac{1}{r\lambda_{\mathrm{a}}} + \frac{1}{r^2}\right) \mathrm{e}^{-\frac{r}{\lambda_{\mathrm{a}}}} (\hat{\sigma}\cdot\hat{r}), \tag{1}$$

where m_{f} is their mass, $\hat{\sigma}$ is the Pauli spin matrix, $\vec{r}$ is the vector between them, and $\lambda_{\mathrm{a}} = h/m_A c$ is the axion Compton wavelength [1, 6], which determines the range over which the interaction extends. The range of interaction can be as small as $\lambda = 30$ μm depending on the mass of the axion [8]. For the QCD axion the scalar and dipole coupling constants $g_{\mathrm{s}}^{\mathrm{N}}$ and $g_{\mathrm{p}}^{\mathrm{N}}$ are directly correlated to the axion mass. Since the axion couples to $\hat{\sigma}$ which is proportional to the magnetic moment $\vec{\mu}_{\mathrm{N}}$ of the nucleus, the axion coupling can be treated as a fictitious 'magnetic field' B_{eff} through an interaction potential

$$U_{\mathrm{sp}}(r) = -\vec{\mu}_{\mathrm{N}} \cdot \vec{B}_{\mathrm{eff}}. \tag{2}$$

In ARIADNE, the fictitious field is generated by a tungsten sprocket. As the teeth of the sprocket rotate past the ^{3}He spin sample, the distance between the tungsten material and ^{3}He spin sample is modulated, thus resulting in a modulation in the field strength seen by the spins.

It is vital to note that such a magnetic field as described in equation (2) does not conform to Maxwell's equations and so cannot be detected directly with a magnetometer such as a superconducting quantum interference device (SQUID) [1]. Instead, the nuclear spins in a hyperpolarized sample of ^{3}He do couple to the locally-sourced fictitious field, and can precess resonantly with the modulation as in a nuclear magnetic resonance (NMR) experiment. This precession allows the fictitious field to be indirectly detected by using an SQUID magnetometer to measure the real magnetic field generated by the precessing ^{3}He nuclear spins [2]. The setup relies on superconducting magnetic shielding, required to screen the ^{3}He sample from ordinary magnetic noise.

For the geometry described in [2] and illustrated in figure 1, the fictitious magnetic field felt at the sample is constrained to be very small, less than 10^{-19} T. Thus experimental sensitivity is paramount. Under ideal operating conditions the sensitivity of the experiment will be limited by quantum projection noise in the sample itself [1]. The sensitivity is thus maximized for a longer transverse decoherence time T_2 of the sample, with the minimum detectable magnetic field scaling as $(nVT_2)^{-1/2}$ where n is the density of polarized spins in a sample of volume V. This minimum detectable field is due to the standard quantum limit from spin projection noise [1, 9], and is expected to be proportional to $1/\sqrt{N}$ for an ensemble of N polarized spins. In practice the experimental sensitivity is constrained by several considerations. The first is ordinary (external) magnetic noise, which would exceed the sub-aT axion signal if unmitigated. A second stems from magnetic field gradients in the sample volume, which result in a Larmor frequency which varies throughout the sample, decreasing the effective T_2. Thirdly, the sample's nuclear Larmor precession frequency (set by the overall magnetic field felt by the sample) and the modulation frequency of the axion field set by the sprocket's rotational frequency must be matched in an experimentally practical way.

The methods presented in this paper may be generally useful for magnetic field control near superconducting boundaries in other experiments where similar considerations apply, even those relying on detecting the cosmological axion field, such as the Casper axion dark matter experiment [10] or the QUAX proposal [11].

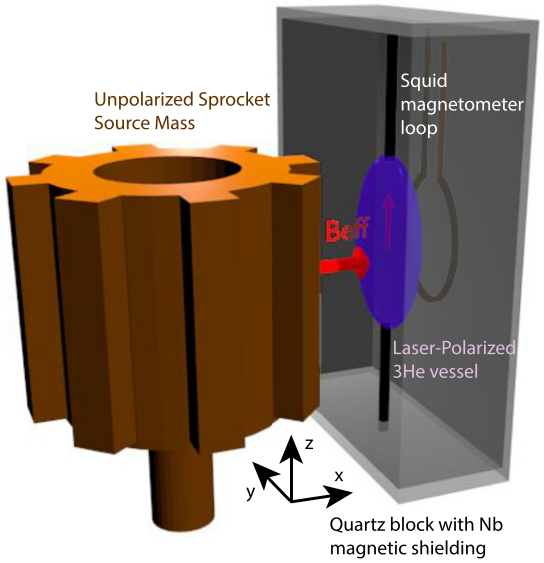

Figure 1. Setup: a sprocket-shaped source mass is rotated so its 'teeth' pass near a laser-polarized ^{3}He NMR sample at its resonant frequency, producing a time-varying 'fictitious' magnetic field via the axion potential. The resulting induced transverse magnetization is read out using an SQUID magnetometer. This distance between the rotating sprocket and He sample is kept within $\approx 200\ \mu$m to search for short-range axion-mediated forces. The sample chamber is embedded in a quartz block coated with thin-film superconducting Nb shielding.

2. Experimental setup and statement of problem

For concreteness, to model the magnetic environment of the magnetized ^{3}He sample near a superconducting (SC) boundary, we choose a particular geometry relevant for the ARIADNE experiment. The sample container is chosen to be an oblate spheroid of dimensions 0.15 mm, 3 mm, and 3 mm in the x-, y-, and z-directions, respectively. A pancake-like shape of the sample chamber allows the He detector volume to remain close to the source mass rotor, within the Compton wavelength of the axion. For simplicity, we assume that the polarization fraction is 1 and the spins are vertically aligned in the z-direction, with a nuclear spin density of 2×10^{21} spins/cc, corresponding to the maximal spin density of the 4.2 K ^{3}He gas considered in the experiment. The reason for the spheroidal shape is to maintain a uniform magnetic field inside the sample and to maximize the signal by having as much volume of the sample region in close proximity to the source mass, as discussed in detail below. The spheroid is embedded in a quartz cube of approximate dimensions 5 cm, coated with a Nb SC film. The quartz thickness between the face of the spheroid and the wall of the cube (in the x-direction) is set to be 75 μm, sufficient to hold vacuum but thin to allow close proximity to the drive mass sprocket.

2.1. Ordinary magnetic noise

At the location of the ^{3}He sample, ordinary magnetic backgrounds can lie at the $10^{-12}\ \frac{\mathrm{T}}{\sqrt{\mathrm{Hz}}}$ level, well above the expected axion signal, if not screened [2]. A primary example of concern is Johnson noise, where thermal motion of electrons in conducting materials produces a spectrum of magnetic field fluctuations near their surface [12]. The presence of such noise in fact necessitates the use of SC shielding surrounding the sample region, since SC materials, being of zero resistance, are immune to such noise. Other examples of backgrounds include magnetic fields due to the magnetization of the rotating source mass sprocket due to the Barnett effect [13], and due to the magnetic susceptibility and any magnetic impurities in the sprocket [2]. However, because the fictitious magnetic field is not subject to Maxwell's equations, it is not screened by SC magnetic shielding [1]. Thus SC shielding can be installed to reduce the ordinary magnetic noise felt by the sample without also reducing the fictitious field signal. However, geometry constraints make perfect shielding nontrivial, as wires for sensors must extend into the shielded region. These constraints, and efforts to characterize (and improve) the shielding factor of the resultant design are described in section 5.

In order for the experiment to achieve design sensitivity, a shielding factor of approximately 10^8 is needed at frequencies of 50–100 Hz [2]. Such shielding factors have been achieved for example with solid Nb SC tubes [14]. The approach described in this paper requires (at least partial) use of thin film SC

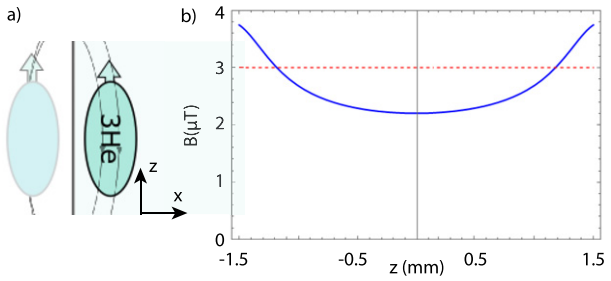

Figure 2. (a) (Not to scale) An illustration of the 'Meissner image' of the spheroidal sample volume. As for a uniformly magnetized sphere, the magnetic field interior to a magnetized oblate spheroid with the magnetization aligned with one of the principal axes is uniform. When abutting a SC surface, the Meissner effect prevents the magnetic flux from penetrating the SC wall. Mathematically this can be treated with the method of images [15]. The arrows indicate the magnetizations of the real and image spheroids, while the lines indicate the magnetic field of the image spheroid, which perturbs the otherwise constant field interior to the real spheroid. (b) Norm of the magnetic field along the z-axis in the spheroid, with a bias field applied of approximately 23 μT opposing the direction of magnetization, tuned to achieve an average Larmor frequency around 100 Hz. The dotted red line indicates the field value without the perturbation introduced by the image spheroid. In this configuration the fractional variation due to the perturbation is up to 26%.

shielding, due to the requirement of very close proximity (a distance of order λ_a or less) between the ^{3}He sample and sprocket mass. Experimental work is in progress to evaluate the efficacy of thin film Nb on achieving such shielding factors in the experiment.

2.2. Bias field control

The ^{3}He sample is characterized by its Larmor frequency $\omega = \gamma B_0$, where γ is the gyromagnetic ratio when the sample is subject to a constant magnetic field B_0. During sprocket rotation, the fictitious magnetic field is modulated on resonance with ω to maximize its effect. To keep the two frequencies as close as possible, both the rotational frequency of the sprocket and the magnetic field felt by the sample ideally are both adjustable. In most cases, Helmholtz coils would be used to create a gradient-free magnetic field to tune the Larmor frequency of the sample. However, the ^{3}He sample must remain as close as possible to the rotating sprocket outside the shield, to keep the value of the fictitious magnetic field relatively high. Therefore, the sample cannot sit on the axis of ordinary Helmholtz coils interior to the shield. A design for solving this problem is described in section 4.

2.3. Inhomogeneous broadening

If the ordinary magnetic field varies significantly from one part of the ^{3}He sample volume to another, it becomes impossible to drive the entire sample on resonance, drastically decreasing the experimental sensitivity and the relaxation time of the ^{3}He. To attain maximum sensitivity for the sample geometry and parameters considered, the magnetic field should not vary within the sample by more than $10^{-11}(\frac{1000\ s}{T_2})$ T, where T_2 is the transverse relaxation time [2].

Perturbations to the otherwise constant magnetic field internal to the spheroidal sample volume stem from multiple sources, but the largest is due to the sample's proximity to the SC shield. In the presence of a magnetized object or a current, superconductors screen transverse magnetic fields with surface currents via the Meissner effect. If the superconductor's boundary is planar (as is the case in this design), the resultant induced magnetic field is identical to that produced by an identically magnetized object 'mirrored' over the boundary. This is known as the 'Meissner image' of the object. The Meissner image of the sample volume is an identically magnetized spheroid, placed equidistant from the SC shield but on the other side. Figure 2 shows this mirroring effect. This image spheroid is evidently external to the real sample; therefore its magnetic field is not constant at the location of the real spheroid [16]. This field produces a significant non-constant perturbation in the magnetic field internal to the real sample, resulting in large magnetic field gradients. Figure 2 shows the significant variation in the internal field when the image spheroid is introduced. A scheme for canceling these gradients is described in section 3.

3. Magnetic gradient compensation

Before it is possible to reduce the magnetic gradients in the sample, the full extent of the problem of magnetic images must be found. The essential problem is that while a planar superconductor acts like a magnetic 'mirror', a general SC enclosure is not so simple. For instance, if a magnetized object is placed between two parallel SC planes, one left and one right, it would seem that a magnetic image of the object

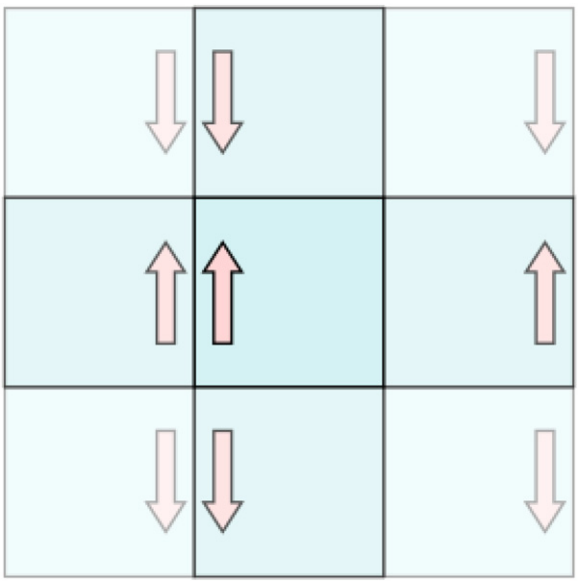

Figure 3. As a result of the 'images of images' phenomenon, a magnetized object in a cubical SC shield experiences a magnetic field that appears as though there is an infinite lattice of such cubes surrounding it.

mirrored across the left plane would cancel the transverse component of the object's field across that plane, and a right-hand image for the right plane. However, the left image's field has a transverse component at the location of the right plane which is not canceled by the right image, and vice versa. Therefore, there must be a 'second order' image, an image of the left image, mirrored over the right plane, and vice versa, to meet the condition of no transverse field. Indeed, these second order images must have their own third order images, etc. Reassuringly, the distance from the real object to the new pair of images increases each time by twice the distance between the planes d, so that the magnetic field between the plates is roughly proportional to $\sum_{n=1}^{\infty} \frac{1}{(2nd)^3}$, which converges. The resulting layout of images can also be generated by 'mirroring' the SC planes across one another, and allowing the resulting image planes to act as magnetic mirrors themselves. This conceptually cleaner approach allows a quick analysis of the cube-shaped SC shield in ARIADNE: the field is the superposition of the field from an infinite 'lattice' of such cubes, each one a mirror image of its neighbors, as illustrated in figure 3.

The benefits of this approach to calculating the magnetic field internal to a SC shield are primarily computational. The placement of images can be calculated to a certain order and then truncated, and the magnetic field of this finite number of identical objects will then approximate the magnetic field produced by surface currents in the superconductor. The spheroid is very close to one side of the cubical shield; therefore the field gradients introduced by the images are dominated by the lowest order and only a few orders need be taken to ensure an accurate approximation. Therefore the method allows for rapid magnetic field calculations, and rapid optimization of the gradient reduction system. In practice, we find that to calculate the effects of induced gradients from the 'Meissner images' of the spheroid at the sub-percent level, it is adequate to consider the field from the magnetized sample itself along with its primary images across each of the six faces of the SC sample volume, and also from the second-order images of the primary images and the third-order images of the secondary images.

The magnetic gradient at the sample location can be influenced and tailored by the addition of other magnetic sources in the interior of the shield. The simplest configuration of such sources is a single SC coil. The axis connecting the centers of the real spheroid and its image is perpendicular to the shield wall and is also an axis of symmetry of the system. Therefore, for a coil to cancel the magnetic field gradients induced by the image it must be located on this axis. There are then only three parameters that can vary: the coil radius, its current, and its location along the axis. A simple algorithm scans the parameter space for the configuration that optimizes some function of the magnetic field across the sample, in progressively finer steps. Two such optimizations were considered: one which minimized the integral of the norm of the magnetic field from the image spheroid across the sample (referred to as field cancellation), and another which minimized the variance of the norm of the total field (referred to as gradient cancellation).

The main advantage of the field cancellation approach is its versatility. If the field perturbation induced by the image spheroid is canceled, the resultant total magnetic field is not only flat (in that its norm does not vary) but also unidirectional, along the magnetization axis. This allows the field to be adjusted to any

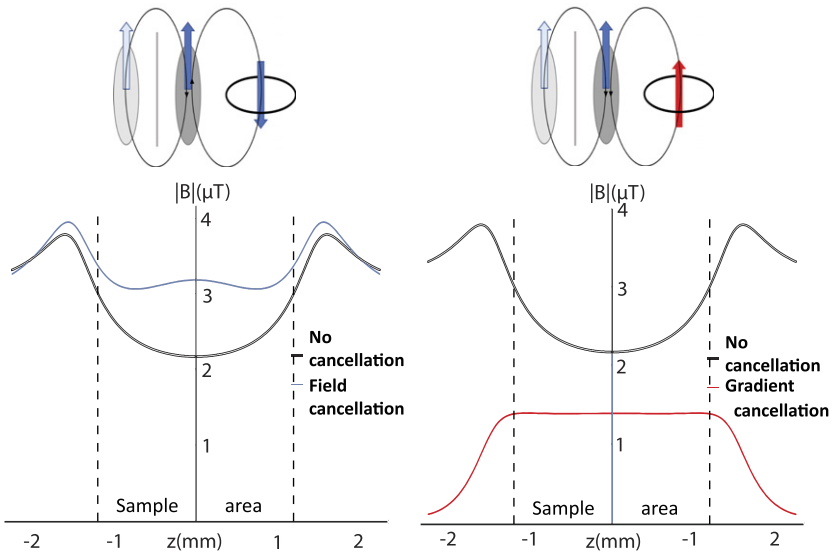

Figure 4. (Left) The field cancellation method seeks to cancel the field from the image spheroid, thereby flattening the total field and allowing it to be tuned to any value. (Right) The gradient cancellation approach seeks to 'flatten' the magnetic field (specifically, minimize the variance of its norm) without regard for its overall value. It reduces the variance by much more than the field cancellation method, but results in a magnetic field which is antiparallel to the spins and nontrivial to tune to an arbitrary value.

level by a set of modified Helmholtz coils (whose design is described in section 4). However, the possible effectiveness of the method is limited, since the perturbed field is bimodal (see figure 2), unlike the field from a coil. This method can reduce the magnetic field variance by a factor of 3, using a 3 mm diameter correction coil carrying a current of 11.6 mA (figure 4).

Rather than attempting to cancel the bimodal perturbed field distribution, the gradient cancellation algorithm finds a different solution. A strong magnetic field opposite the magnetization direction, which falls off gradually at approximately the same rate as the perturbed field, can 'fill in' the central gap in the field. By this method the magnetic field variance can be reduced by a factor of 10^2 or greater, depending on manufacturing tolerances, using a 3 mm coil carrying 1.6 A of current (figure 4). The drawbacks of this approach are that the resultant field, though it has an approximately constant norm, does not have a constant direction. Therefore, if one attempts to tune the field value with Helmholtz coils, the result will not necessarily still be flat, as the angle between the flattened field and the tuning field may vary from one part of the spheroid to another. Furthermore, the prevailing direction of the flattened magnetic field is antiparallel to the magnetization axis of the spheroid. This restricts measurement times to the relaxation time T_1; however, this time can be made extremely long (on the order of hundreds of hours) for optically pumped helium in cesium-coated glass containers [17]. Both the field cancellation and the gradient cancellation coils will be installed in ARIADNE's final design.

4. Bias field control

Conventional NMR experiments employ Helmholtz coils to tune the magnetic field felt by the polarized sample, and therefore its Larmor frequency, to a predetermined value. However, since the distance from the ^{3}He spheroid to the nearest SC boundary is less than the length of its major axis, there is not enough room for a conventional set of Helmholtz coils on the magnetization axis of the spheroid. Furthermore, any set of coils placed on the magnetization axis will induce magnetic images of themselves across the nearby boundary, potentially inducing further magnetic field gradients in the sample. The novel layout shown in figure 5 solves both problems. A semicircular, or 'D' shaped coil is placed with its straight side facing the SC boundary. The resultant Meissner image completes the outer, circular portion, while its straight side provides an equal but opposing current very nearby that of the real straight portion, approximately canceling its magnetic field. The sum of the magnetic fields of the real 'D' shape and its image then approximates that of a circular coil, with the same radius as the semicircle and centered at the SC boundary. The approximation improves the closer the straight side of the semicircle is brought to the boundary—in practice they will be as close as manufacturing tolerances allow. By this approach, large Helmholtz coils can be approximated nearby SC boundaries, and since the Meissner image across the nearby boundary forms a part of the Helmholtz field there are no image-induced magnetic field gradients.

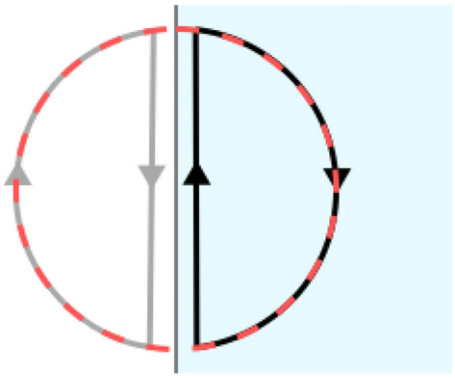

Figure 5. The 'D coil' design employs the Meissner image (gray) of the real, 'D' shaped coil (black) to approximate the field of a Helmholtz coil, represented by the dotted red circle.

By analogy with the 'lattice of cubes' view of the total magnetic field of a source in a cubical SC shield (figure 3), the field of a 'D coil' inside a cubical shield approximates that of an infinite lattice of rectangular prisms. The prisms have side lengths equal to that of the cube on two sides and twice that of the cube along the axis normal to the side of the cube over which the 'D coil' is reflected, and each one contains a full circular coil halfway along the long side of the prism, each a mirrored copy of its neighbors. This approximation allows for rapid, analytic calculations of the total field from the 'D coils' and all their images, and investigation of how those images affect the Helmholtz field. Then the parameters of the Helmholtz and cancellation coils can be optimized, after which the optimal configuration is subject to finite element analysis using COMSOL multiphysics software.

One consequence of the lattice of images of the Helmholtz coils is a change in the usual requirement that the distance between the coils is equal to their radius. In the case of 'normal' Helmholtz coils, the condition ensures that the second directional derivative of the norm of the magnetic field along the axis of the coils vanishes at the center. However, when the images of the coils are included, this derivative becomes nonzero. To again minimize the derivative, the distance between the coils must be slightly increased. The necessary change is greater the larger the coils are, because larger coils are farther apart and therefore closer to the walls of the SC shield. For example, 2 cm coils must be moved apart an extra 0.4 mm to compensate for the image fields, while 3 cm coils must be set apart 4 mm extra, in a box of dimensions 5 cm per side.

5. Magnetic shielding design considerations

5.1. Quartz block design with integrated sensors and magnetic field control

The quartz ^{3}He sample chamber cavity is fabricated by fusing together two pieces of quartz containing hemi-spheroidal cavities. After this, other blocks of quartz with patterned Nb wires are epoxied to the block containing the ^{3}He cell, and the entire assembly will be coated with approximately 1.5 μm of Nb metal, as shown in figure 6. Depending on the film quality, this thickness is chosen to be a sufficient number of penetration depths to provide adequate shielding performance, subject to constraints from film adhesion. Experimentally we have achieved good adhesion of Nb films of thickness ranging from 250 nm to 1.5 μm on quartz substrates, as reported in section 6. However, the SQUID used to measure the magnetic field of the ^{3}He must be powered, and its signal read out, by wires. These wires must therefore exit the SC shield. Additionally, ^{3}He plumbing must pierce the shield so that the hyperpolarized helium can enter the sample volume. There must therefore be holes in the shield (see figure 7), resulting in a reduced shielding factor. COMSOL [18] multiphysics software was used to characterize the shielding factor, and to develop an understanding of its dependence on design geometry.

Initial COMSOL simulations calculated the shielding factor of a cube with a single uncapped tube extending from one side. It was found that the resultant interior field depended strongly on the angle between the applied exterior field and the axis of the cylinder. This phenomenon is explained physically by the fact that surface currents running in the azimuthal direction around the tube can effectively cancel an axial magnetic field, while there is no complete planar path for current to travel with the axis of the tube in-plane. External fields transverse to the axis of the tube are therefore screened less effectively. For a 15 mm long tube with a 3 mm diameter, screening was of order 10^{15} for a longitudinal magnetic field (along the cylinder axis) and 10^{13} for one transverse to the axis. Further simulations calculated the shielding factor of a

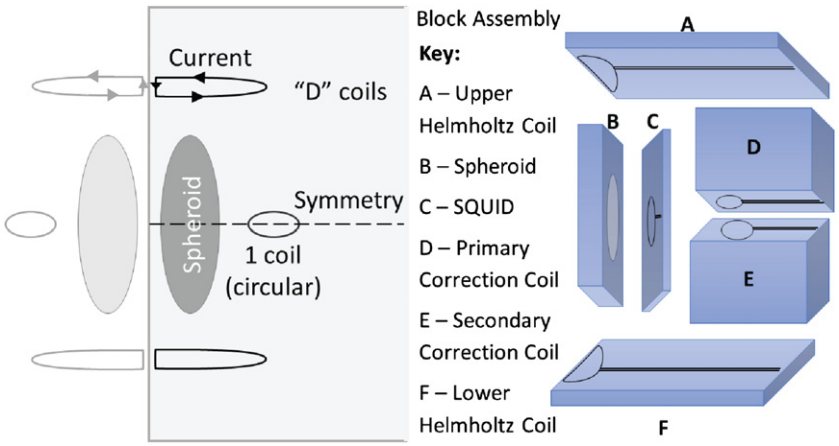

Figure 6. Schematic of quartz block construction prior to Nb coating, showing ^{3}He sample block as well as patterned coils on additional quartz sections for SQUID readout, magnetic bias field control, magnetic gradient control, and magnetic calibration testing.

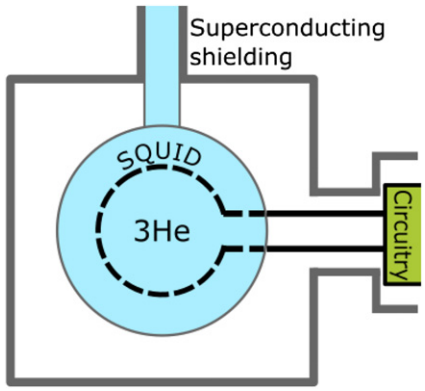

Figure 7. A schematic view of the SC shield around the ^{3}He sample, showing the necessary holes, which limit the shielding factor. Openings in the shield are required for filling the sample chamber with ^{3}He gas as well as for applying and receiving electrical signals.

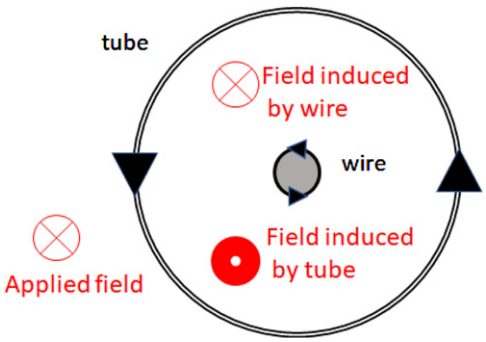

Figure 8. A cross-sectional view of the current (black arrows) and magnetic field (red vectors) inside a SC tube with a central SC wire in an applied magnetic field. Since the shielding from the tube is imperfect, an azimuthal current is induced in the surface of the wire, resulting in a worse shielding factor in the vacuum between the wire and the tube.

SC cube with two holes, located on adjacent sides (90 degrees apart), and found that it was not significantly worse than the transverse field shielding factor of a block with a single hole.

An important consideration in the calculation of the shielding factor of the SC enclosure is the effect of the signal wires themselves. There is a topological difference between the cross-section of an empty SC tube (where the interior vacuum is simply connected) and that of a tube with a central SC wire inside (where the vacuum is not simply connected), whose design mirrors that of a coaxial cable. As a result, even small

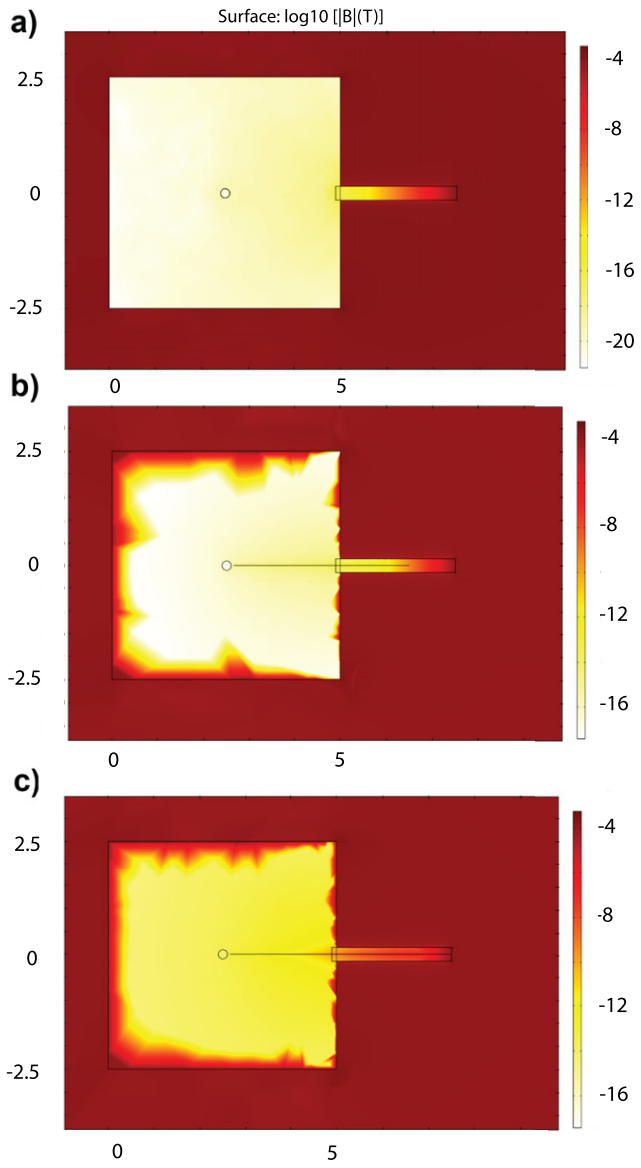

Figure 9. Finite element simulation of the magnetic field along the axis of the tube emerging from the SC shield, where the length of the SC portion of the central wire is varied from no SC wire, to one that extends to a point 10 mm from the end of the tube, to one that extends to the end of the tube. Dimensions shown are in cm. The applied field is 100 μT in the z direction (toward the top of the page in the images). The shaded color bar displays the $\log_{10}$ value of the norm of the magnetic field in Tesla.

diameter central wires induce a large change in the shielding factor of the tube. Figure 8 shows the physical process (i.e. the current density) by which a central SC wire reduces the shielding factor. In effect, the residual (non-screened) magnetic field inside the tube induces azimuthal surface currents in the wire. By Lenz's law, these currents reduce the magnetic field inside the wire, but therefore they must increase the magnetic field in the space between the wire and the tube (since the external magnetic field of a finite solenoid is opposite to its internal field). Figure 9 shows that for an applied transverse magnetic field, the presence of the central SC conductor significantly degrades the shielding factor of the geometry. Here we compare the cases of a central superconductor which extends along the entire tube length, one that extends along part of the tube length, and the case with no central SC wire.

When the central SC wire is included in our simulations, the shielding factor of the single-tube shield drops to of order 10^6 for both a magnetic field parallel to the cylinder axis and for a transverse field. As figure 9 shows, the greater the length of SC wire present, the less shielding is achieved. However, the difference between the case with 15 mm of SC wire in the tube and that with no superconductor at all is comparatively small, suggesting that reducing the length of superconductor could be an effective strategy to recover high shielding factors.

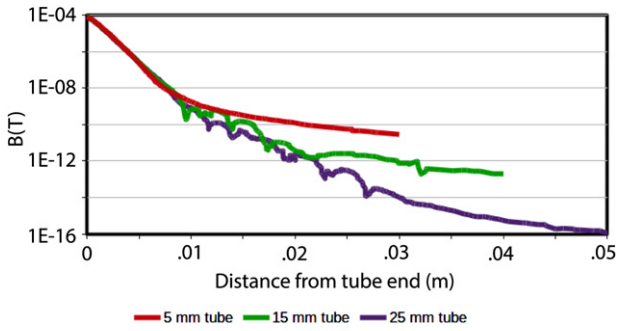

Figure 10. Finite element simulation of the magnetic field along the axis of the tube emerging from the SC shield, as a function of distance from the tube end. Tube lengths between 5 mm and 25 mm are plotted. An external field of 10^{-4} T is applied transverse to the tube.

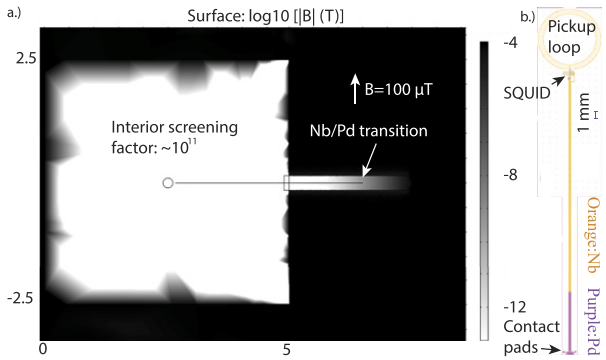

Figure 11. Left: a numerical simulation of the magnetic shielding factor of the pierced shield, including the SC SQUID. Distances shown are in cm. The applied field is 100 μT for this simulation. The shaded color bar displays the $\log_{10}$ value of the norm of the magnetic field in Tesla. Right: the design of the SQUID to be used in ARIADNE.

Two practical approaches are used to improve the shielding factor. Firstly, simply increasing the ratio of the tube's length to its diameter increases the shielding factor. For a tube which is open on both ends, axial magnetic fields are suppressed at the center of the tube exponential in the length-to-diameter ratio [19]. For example, our simulations show that increasing the tube length from 5 mm to 25 mm results in a factor of 10^5 improvement in the shielding factor (figure 10).

Another method of increasing the shielding factor is to fabricate the central wire from a mix of materials: SC metal for the part closest to the SQUID, and 'normal' (i.e. non-SC) metal for the remainder of the length of wire. At the relatively low frequency ($\sim$ 100 Hz) of ARIADNE's search, normal metals have little to no magnetic shielding properties, so the shielding factor is not significantly reduced by a central wire made of normal metal. However, Johnson noise has the potential to drown out the small fictitious magnetic field if any normal metal is placed too close to the SQUID and inside the shield. There is therefore an ideal length of superconductor, which balances the reduction of Johnson noise with the maximization of the shielding factor.

The design chosen for ARIADNE is indicated in figure 11, where the central conductor changes from SC Nb to normal metal Pd 15 mm from the block in the 25 mm tube, and exhibits a predicted shielding factor of approximately 10^{11}, which should be approximately 3 orders of magnitude greater than that needed to achieve the design sensitivity.

6. Experimental tests of thin-film niobium superconducting shielding

The exterior of the quartz block containing the ^{3}He sample shown schematically in figure 6 will be coated with a thin film of niobium to act as a SC shield. To eliminate magnetic gradient noise due to vibration [2], the film will ideally be deposited directly on the quartz block to take advantage of the mechanical stiffness of the block, rather than relying on a free standing SC foil. While solid Nb has been shown [21] to provide shielding factors in excess of 10^8, here we investigate the shielding performance of sputtered thin-film Nb on a quartz substrate. We study deposition on a cylindrical substrate of two different aspect ratios and for a

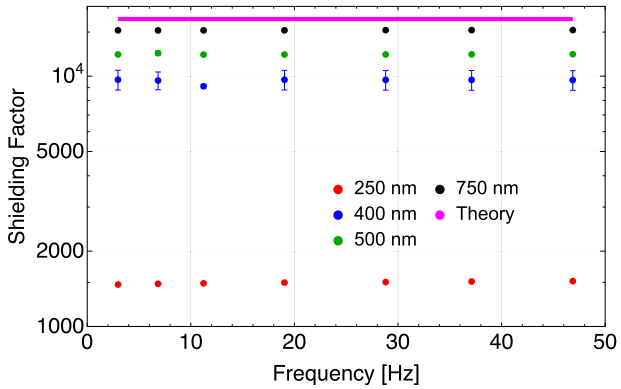

Figure 12. Measured shielding factor for Nb-coated quartz tubes with a diameter of 25 mm compared with the theoretical value [20] for a perfect superconductor. The tube lengths were $L = 148.7 \pm 1$ mm due to the machining error. The theoretical estimation considered a 7.5 mm offset of the SQUID position from the center of the tube.

variety of film thicknesses. The cylindrical geometry is not intended to reproduce the quartz sample block itself, but is relevant for evaluating the quality of the shielding film and for modeling the extension tubes to be affixed to the quartz block.

We prepared sputtered Nb on quartz tubes of length 150 mm with diameter 14 mm and 25 mm. The Nb sputtering chamber was evacuated to a pressure ranging from 5×10^{-8} Torr to 1×10^{-7} Torr prior to Nb deposition and the quartz was pre-cleaned with solvent and degreaser, resulting in excellent adhesion of the Nb film. Deposition thickness was studied between 250 nm and 1500 nm, and the SC transition temperature of the Nb films was studied using mutual inductance measurements and found to range between 7.62 and 8.28 K. We also found a variation in T_c at different positions along the tubes, showing that during the deposition process, the Nb has been unevenly affected by oxygen degradation. A new sputtering setup employing cleaner ceramic holders has been fabricated and is being tested for future improvements.

The 25 mm tubes were used to ascertain dependence on thickness for the shielding factor of the Nb thin films. Due to its aspect ratio, the tube with larger diameter is expected to have poorer shielding factor performance ($< 1.7 \times 10^4$). Using an external Helmholtz coil, a transverse uniform field of 100 μT was applied in a shielded room in order to measure the shielding factor as measured by an SQUID magnetometer inside the Nb coated tube. For the shielding factor measurement, we prepared a movable SQUID probe (CE2Blue shunted current sensor [22]) inside of a hollow G10 tube which inserts into the larger Nb-coated quartz tube. For each sample tube, the magnetic field strength inside the tube and outside of the tube were measured by adjusting the SQUID position and input coil position. The results are shown in figure 12, and indicate that for 750 nm Nb thickness the film is able to attain close to the theoretical value for a perfect superconductor with this geometry, considering geometrical uncertainties including the variance of tube length among the samples with average length $L = 148.7 \pm 1$ mm and the 7.5 mm offset of the SQUID position along the axis of the tube from the tube center.

For testing the tube with smaller (14 mm) diameter which provides a larger shielding factor end entails measuring smaller magnetic fields, to prevent the misalignment between the SQUID and the external field source, the position of the SQUID and the external magnetic field source inside the Dewar has been fixed. The figure 13 shows the diagram and picture of the shielding factor measurement setup used for the 14 mm tube. A hole in the G10 tube enables monitoring the position of the SQUID. On the outside of the hole, the dipole coil with diameter 6.3 mm and 11 turn is placed to apply an external magnetic field to the SQUID. For comparison we prepared two lead shields made of 0.2 mm foil: one having a single layer of lead foil with a soldered seam and another having three layers of lead foil to prevent the penetration of external field through the seam. Their diameter was about 1.4 mm smaller than Nb coated quartz samples, so that the rolled foil could be inserted inside of the quartz tube. We conducted all measurements in a magnetically shielded room.

First, we calibrated the dipole field and SQUID. A commercial current sensor (CE2blue) [22] with shunted input was used as the SQUID magnetometer with pick up loop area $A = 1$ mm^2 and input coil inductance $L_{in} = 0.42$ μH. The SQUID electronics sensitivity was set for $V/\phi_0 = 592$ mV/ϕ_0, where ϕ_0 is flux quanta. With the external magnetic field generated by the dipole source using a signal generator, the SQUID signal was measured using a spectrum analyzer (SRS SR770). To check the sensitivity, using Biot–Savart law, the magnetic field applied to the pickup loop region was estimated to be 85 nT with $0.2V_{pp}$

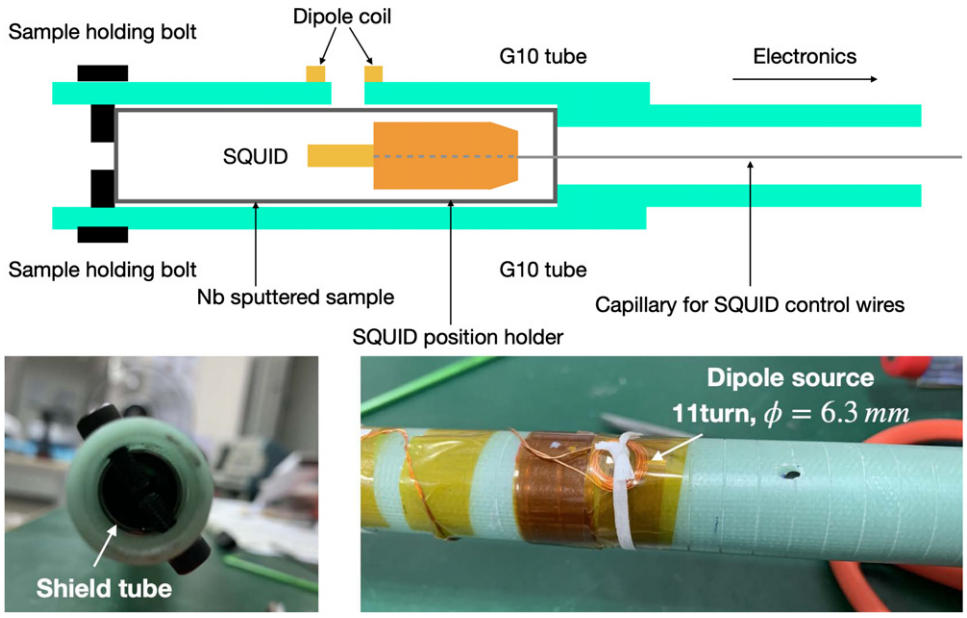

Figure 13. (Upper) Schematic and (lower) photograph of shielding factor measurement apparatus using an SQUID magnetometer. SQUID sensor and dipole source coil position are shown for the 14 mm diameter quartz tube.

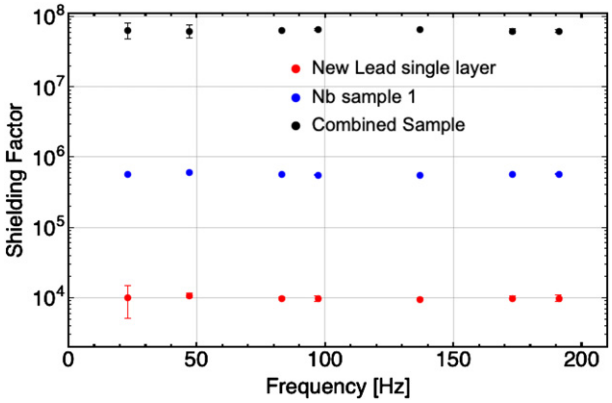

Figure 14. SF for single-layer lead shield with diameter 11 mm and length 150 mm, (red); 750 nm thickness of Nb film on sample 1 (14 mm diameter, 150 mm long quartz tube), (blue); combined lead and Nb sample, (black). Theoretical SF [20] for a solid Nb tube of this dimension is 10^8.

applied. Assuming magnetic field B_0 is uniform over the small pickup loop area, the current in the pickup loop $I_{\text{in}} = B_0 A/L_{\text{in}} \approx 20\ \mu\text{A}$. The CE2blue sensor has input coil-SQUID coupling $1/M_{\text{in}} = 0.25\ \mu\text{A}/\phi_0$. Thus we estimate the SQUID injection flux $\phi_{\text{s}} = \phi_{\text{s}} = \frac{B_0 A/L_{\text{in}}}{1/M_{\text{in}}} \approx 0.78\phi_0$. The SQUID measures the magnetic applied flux as $\phi_{\text{s}} = 420\ \text{mV}/(592\ \text{mV}/\phi_0) \approx 0.71\phi_0$, yielding reasonable agreement.

The expected shielding factor (SF) of a cylinder with transverse external field can be estimated as $\text{S.F} = \cosh 1.84z/a$, where z, a are height and diameter of the cylinder [20]. The ideal SF for our given geometry ($z = 150$ mm, $a = 14$ mm) is approximately 10^8. This ideal case is based on an assumption in which the surface is a perfect superconductor and the magnetic field is applied uniformly. In the case of the 14 mm tube, however, the magnetic field was applied by the small dipole near the surface of the tube, therefore the situation differs from the ideal case.

With $10V_{\text{pp}}$ applied voltage to dipole, we measured the dipole signal for a tube with 750 nm of Nb deposited after evacuating the sputtering chamber to 5×10^{-8} Torr. We also measured the signal for the single-layer Pb foil, and the Nb + Pb combined sample. Figure 14 is the measured SF result for Nb, Pb, and Nb + Pb samples. Measurements are reported up to frequencies of 200 Hz, which includes the relevant

target operating range for ARIADNE (50–100 Hz). We find the SF is independent of frequency below 300 Hz for all of the samples studied. A frequency-dependent parasitic signal was observed over 300 Hz. We assume that this parasitic signal at higher frequencies comes through the capacitive coupling between the cables and circuits.

The SF of Nb sample was measured as 5×10^5. SFs of other 750 nm Nb-coated tubes were approximately 3 times worse when measuring tube samples deposited with higher initial chamber pressures in the 10^{-7} Torr range, indicating greater impurities. The lead one-layer shield by itself shows a SF of 10^4, probably because the slit was not perfectly soldered. For reference, the triple layer lead foil indicated an SF of approximately 2×10^6 (not shown in figure 14). The SF of the combined one-layer foil and Nb-coated sample was measured as 6×10^7, within a factor of 2 of the theoretically expected result for a perfect superconductor with this geometry. The results obtained so far suggest that improved sputtering deposition conditions may lead to even greater SFs for this geometry, but that when combined with Pb foil, the attained SFs are already sufficient to allow operation of the ARIADNE experiment at or near its design sensitivity.

7. Conclusion

We have presented a method to control the magnetic field and gradients within a gaseous sample of polarized nuclear spins in close proximity to a SC boundary. We have analyzed shielding solutions using finite element simulation. The approach could be used for other precision NMR or electron-spin resonance (ESR) studies in the neighborhood of a SC boundary [10, 11, 23]. We have also experimentally tested the magnetic SF of thin-film SC Nb deposited on a quartz substrate and find that thin-film niobium of suitable thickness, when utilized in combination with thin lead foil, can provide adequate performance for the ARIADNE experiment to attain its ultimate design sensitivity.

Adequate magnetic shielding is essential to achieve quantum projection-noise limited sensitivity in NMR- and ESR-based fifth-force searches and dark matter haloscope experiments. Future prospects for improvements in the search for novel spin dependent interactions could include investigations with a spin polarized source mass, or improved sensitivity with new cryogenic or quantum technologies. Spin squeezing or coherent collective modes in ^{3}He could offer prospects for improved sensitivity beyond the standard quantum limit of spin projection noise in experiments such as ARIADNE, potentially allowing sensitivity all the way down to the SQUID-limited sensitivity (dashed-dotted line in figure 1 of reference [2]). This would allow one to rule out the axion over a wide range of masses, and when combined with other promising techniques [10, 24, 25], and existing experiments [7, 21] already at QCD axion sensitivity, could allow in principle the QCD axion to be searched for over its entire allowed mass range. Methods to mitigate magnetic field noise and unwanted magnetic gradients are essential to realize the full potential of these techniques.

Acknowledgments

We thank A Arvanitaki, B Cabrera, B Halperin, and K Irwin for discussions, and H Mason for early assistance with numerical simulation work. This work is partially supported by the US National Science foundation, Grants PHY-1509176, 1510484, 1506508, 1806671, 1806395, and 1806757. Part of this work is supported by Institute for Basic Science under Grant No. IBS-R017-D1-2021-a00. A Reid, J C Long, W M Snow, C-Y Liu, J Shortino, and I Lee acknowledge support from the Indiana University Center for Spacetime Symmetries.

Data availability statement

The data that support the findings of this study are available upon reasonable request from the authors.

ORCID iDs

A A Geraci https://orcid.org/0000-0001-7009-0118
D Kim https://orcid.org/0000-0002-4097-2889

References

[1] Arvanitaki A and Geraci A A 2014 *Phys. Rev. Lett.* **113** 161801
[2] Fosbinder-Elkins H *et al* 2018 Progress on the ariadne axion experiment *Microwave Cavities and Detectors for Axion Research* eds G Carosi, G Rybka, K van Bibber (Berlin: Springer) pp 151–61
[3] Peccei R D and Quinn H R 1977 *Phys. Rev. Lett.* **38** 1440–3
[4] Weinberg S 1978 *Phys. Rev. Lett.* **40** 223–6
[5] Wilczek F 1978 *Phys. Rev. Lett.* **40** 279–82
[6] Moody J and Wilczek F 1984 *Phys. Rev.* D **30** 130–8
[7] Du N *et al* 2018 *Phys. Rev. Lett.* **120** 151301
[8] Beringer J *et al* (Particle Data Group) 2012 *Phys. Rev.* D **86** 010001
[9] Budker D and Romalis M 2007 *Nat. Phys.* **3** 227–34
[10] Budker D, Graham P W, Ledbetter M, Rajendran S and Sushkov A O 2014 *Phys. Rev.* X **4** 021030
[11] Barbieri R, Braggio C, Carugno G, Gallo C S, Lombardi A, Ortolan A, Pengo R, Ruoso G and Speake C C 2017 *Phys. Dark Universe* **15** 135–41
[12] Varpula T and Poutanen T 1984 *J. Appl. Phys.* **55** 4015–21
[13] Barnett S J 1915 *Phys. Rev.* **6** 239–70
[14] Hinterberger A, Gerber S and Doser M 2017 *J. Instrum.* **12** T09002
[15] Kordyuk A A 1998 *J. Appl. Phys.* **83** 610–2
[16] Tejedor M, Rubio H, Elbaile L and Iglesias R 1995 *IEEE Trans. Magn.* **31** 830–6
[17] Heil W, Humblot H, Otten E, Schafer M, Sarkau R and Leduc M 1995 *Phys. Lett.* A **201** 337–43
[18] COMSOL Multiphysics, COMSOL, Inc. 2021 https://www.comsol.com
[19] Thomasson J W and Ginsberg D M 1976 *Rev. Sci. Instrum.* **47** 387–8
[20] Claycomb J R and Miller J H 1999 *Rev. Sci. Instrum.* **70** 4562–8
[21] Zhong L *et al* 2018 *Phys. Rev.* D **97** 092001
[22] Supracon AG 2021 CE2blue SQUID sensor http://supracon.com/en/ce2blue.html
[23] Crescini N, Braggio C, Carugno G, Falferi P, Ortolan A and Ruoso G 2017 *Nucl. Instrum. Methods Phys. Res.* A **842** 109–13
[24] Ouellet J L *et al* 2019 *Phys. Rev. Lett.* **122** 121802
[25] Silva-Feaver M *et al* 2017 *IEEE Trans. Appl. Supercond.* **27** 1400204